# Computerized Simulation and Parameterization of a New High-Performance Tubular Solar Collector

F. L. Lansing and C. S. Yung
DSN Engineering Section

*This work is the second of two reports describing the thermal analysis, computerized performance, simulation and performance sensitivity of the new General Electric vacuum tube solar collector. The collector is considered a potential candidate for future DSN solar heating and cooling applications. The first report presented details of the two-dimensional thermal model of the solar collector at steady state. In this report, the second phase of the study is presented to include the computer simulation and the performance parameterization. Comparison of the simulated performance with the manufacturer's test data showed good agreement at wide ranges of operating conditions. The effects of nine major design and performance variables on the performance sensitivity were presented. The results of this parameterization study were supportive in detecting the areas of design modifications for performance optimization.*

## I. Introduction

The high-performance low-concentration tubular solar collector recently manufactured by General Electric Company has been under investigation in the DSN Engineering Section for possible use in future heating/cooling applications at the ground stations. The thermal performance of this collector was not sufficiently reported by the manufacturer, although high performance was claimed. Details of the in-house two-dimensional thermal analysis and the mathematical model were previously reported in Ref. 1 as a first phase of the investigation.

In order to support the second phase of the investigation, which is the parameterization of the collector and the numerical evaluation of its performance, an in-house computer program has been written using the mathematical model developed in Ref. 1. Appendix A gives the details of the computational sequence followed. Furthermore, in order to validate the performance, improve the present design, and search for the dominant parameters that affect the performance, a sensitivity analysis is needed. This article focuses on the second phase of the study and reports on the results obtained from this sensitivity analysis.

Only few experimental data were supplied by the manufacturer (see Refs. 2 and 3), and therefore the results of the performance simulation will be compared against these test data only. Some unknown material properties, physical dimensions and boundary conditions were assumed in this work to complete the modelling process as will be described in detail later.

## II. Collector Description

Two versions of the collector design have been manufactured by G.E. Both versions have the same basic features, with the exception of a few differences explained as follows. The detailed description of the basic features of the collector was given in Ref. 1, but is briefly mentioned here for convenience. The collector module consists of a number of heat collection units: 10 in the first version and 8 in the second. The units are mounted in parallel with a highly reflective back reflector. The back reflector is a V-shaped surface in the first version as shown in Fig. 1. In the second version, the back reflector is a double cusp (parabolic shape) as shown also in Fig. 1. Each unit contains a U-shaped copper tube and the tubes of the units are connected in series to form a serpentine. Each collector unit consists of two coaxial cylindrical glass tubes with evacuated annular space in between.

The first (outer) cylinder serves as a "window," and the second (inner) cylinder is selectively coated on the outer surface to serve as the "absorber." The heat is transferred through the second glass tube to a conforming cylindrical metallic shell made of copper. The latter transfers the heat to the working fluid passing through the U-tube. To allow for thermal expansion, one side of the U-tube is attached to the copper shell while the other side is left free to move as shown in Fig. 1. The thermal model, however, considers that both sides of the U-tube are in contact with the copper shell.

Although the second version of the collector design was made public after the mathematical model was established in Ref. 1, the first design will still be analyzed. The differences between the two designs, namely, the shape of the back reflector and the number of units per module, will not be changed in the thermal model.

## III. Additional Assumptions

In addition to the assumptions and idealizations that were made to simplify the collector simulation in Ref. 1, the following assumptions are added in the second phase of the study for completeness.

(1) The outer surface of the second glass tube is assumed to be selectively coated, instead of coating the outer surface of the metallic shell. This will reduce the outward long-wave radiation losses to the first glass tube.

(2) The deformation, due to lateral thermal expansion of the U-shape tubing, is assumed to be insignificant and not to cause any glass breakage. Also, the present slit suggested by the manufacturer in the metallic shell is assumed to be narrow enough to keep the cold and hot fluid tubing always in contact with the shell. This assumption is made to increase the fin efficiency and improve the heat transfer between the fluid and the copper shell.

The above assumptions, together with the thermal model presented in Ref. 1, were used to construct a computer program as shown in Appendix A. An illustrative example on the use of the computer program in determining the various performance characteristics is given in Appendix B.

## IV. Comparison with Experimental Tests

In order to provide a cross-checking on the computer program validity, a comparison is made of some simulated performance results against the manufacturer test data. The dotted line in Fig. 2 was provided by the manufacturer (in Ref. 3), based on experimental tests made in 1978 at Desert Sunshine Exposure Tests, Inc., and Florida Solar Energy Center, using a collector module of the first design version. The X points in Fig. 2 are the simulated results of some arbitrarily selected operating conditions having different inlet fluid temperature $T_c(0)$, ambient temperature $T_A$, and solar intensity $I$. The abscissa in Fig. 2, $[T_c(0) - T_A]/I$, is commonly chosen to compare solar collectors of different optical and thermal characteristics. The coordinates of Fig. 2 also fit Eq. (A-36), in Appendix A, where the ordinate intercept represents the optical efficiency and the curve slope is an indication of the thermal losses to the ambient.

The collector characteristic equation can be expressed, from Fig. 2, by the approximate formula:

$$\eta_{\text{module}} = 0.640 - 2.0669 \frac{T_c(0) - T_A}{I} \qquad (1)$$

where the temperatures $T_A$ and $T_C(0)$ are in degrees Celsius and $I$ is in W/m$^2$.

The good agreement between the computer simulation results and the experimental tests, indicated in Fig. 2, provided the validation needed for the computer program. Consequently, the performance sensitivity to nine major variables was done next using a baseline set of operating conditions. The numerical example presented in Appendix B gives the magnitude of this set of variables used as a baseline. The flow rate of a collector module (10 collector units) was chosen to be 50 kg/h (instead of 5 kg/h used in Appendix B) to follow the manufacturer's specification. The simulated module efficiency, at the reference conditions, is 49.47%, corresponding to (1) a solar radiancy I of 630.7 W/m$^2$, (200 Btu/h ft$^2$), (2) a wind speed $W$ of 4.47 m/s, (3) an ambient temperature $T_A$ of 4.4°C

(40°F), (4) a reflectivity of absorber shell $b$ of 0.5, (5) a second glass tube emissivity, $\epsilon_s$ of 0.2, (6) a reflectivity of back reflector $\rho_v$ of 0.9, (7) a U-tube size of 6 mm (1/4 in.) nominal diameter, (8) a fluid mass flow rate $M$ of 50 kg/h, and (9) an inlet fluid temperature to the first collector unit $T_c(0)$, of 48.89°C (120°F). The selection of these reference conditions was made using explicit and implicit data provided by the manufacturer.

## V. Performance Parameterization

The performance of the collector is mainly determined by the above nine major variables. Each variable is set to change in value around the preselected reference state, and the results of one collector module (10 units) are discussed in the following subsections.

### A. Effect of Solar Radiancy Variations

The performance sensitivity to the solar radiancy $I$ is plotted as shown in Fig. 3. A nonlinear relationship is evident between the radiancy vs the fluid temperature gain or the collector efficiency. An increase of the solar intensity by 50%, for example, will improve the fluid temperature gain by 63.8% and the collector efficiency by 9.21%. On the other hand, a 50% reduction of the solar intensity will lower the fluid temperature gain by 60.9% and the collector efficiency by 27.9%. This behavior can be best explained by using the efficiency expression Eq. (A-36) in Appendix A. The efficiency of one collector unit given in Eq. (A-36) is divided into two terms. The first term

$$\left[F\lambda\left(\alpha_{a,e}+\alpha_{f,e}\,\frac{B_4}{B_7}+\alpha_{s,e}\,\frac{B_6}{B_7}\right)\right]$$

which is independent of the intensity $I$, represents the optical efficiency of the collector at zero thermal losses. The second term, namely,

$$FB_0\,[T_c(0)-T_A]/I$$

herein called the thermal loss factor, is proportional to the temperature difference $(T_c(0)-T_A)$ and inversely proportional to the intensity $I$. This finding explains the nonlinear relationship of the efficiency vs the intensity as illustrated in Fig. 3. In addition, Eq. (A-36) can be used to interpret the increase of collector efficiency when the solar intensity increases.

### B. Effect of Wind Speed Variations

The convective loss coefficient, $H_{fA}$ between the first (outer) glass tube and ambient air is solely a function of the wind speed as given by Eq. (A-12) in Appendix A. Two extreme values of the wind speed were assumed to take place around the reference state. The first is a no-wind condition and the second is a wind speed of 8.94 m/s (20 mph), which is double the reference speed of 4.47 m/s (10 mph). The results are plotted in Fig. 4. It is evident from Fig. 4 that the effect of wind speed variations on efficiency and fluid temperature gain is small. At the no-wind condition, for example, the wind velocity decreased by -100% compared to the reference point and caused an increase in the efficiency by only 1.8%. On the other hand, at double the reference wind speed, an efficiency decrease of 0.4% was found. These findings lead to the conclusion that the collector performance has a very small sensitivity to variations in wind speed.

### C. Effect of Ambient Temperature Variations

The effect of ambient temperature was investigated by varying the ambient temperature from -23.33°C (-10°F) to 48.89°C (120°F) around the reference state, which is 4.4°C (40°F), keeping all other parameters the same. The results are plotted in Fig. 5, showing the effects on the collector efficiency and the fluid temperature gain.

Increasing the ambient temperature causes an increase in the collector efficiency due to the reduction of the thermal losses and vice versa. These thermal losses are proportional to the temperature difference $(T_c(0)-T_A)$ as given by Eq. (A-36). An increase of the ambient temperature from 4.4°C (40°F) to 48.89°C (120°F), i.e., an increase of the absolute temperature by 16%, caused an increase in the thermal efficiency by about 28%. This is equivalent to a sensitivity of about 1.75. On the other hand, a decrease of the ambient temperature from 4.4°C (40°F) to -23.33°C (-10°F), i.e., a decrease of the absolute temperature by 10%, caused a decrease in the thermal efficiency by about 12%. Again, the sensitivity to ambient temperature is 1.2, which shows the important role that the ambient temperature plays in the performance.

### D. Effect of Absorber Shell Reflectivity *b*

The optical properties of the metallic shell and the second (inner) glass tube should be carefully selected in the design in order to yield a good collector performance. The mechanism by which the solar energy is absorbed, converted into heat, and transmitted to the working fluid can be one of two types.

The first heat transfer mechanism could be achieved by adopting a heat-absorbing glass material for the second glass tube to act as the "absorber" from which the net absorbed heat is conducted to the metallic shell that holds the fluid tubing. This mechanism is already used by the manufacturer, and it requires that the first (outer) glass tube function only as a "window" for minimizing the outward infrared radiation losses.

Another heat transfer mechanism is envisioned in which both the first and second glass tubes act as a double-paned "window" made of common clear glass with negligible heat absorbing capability. The major portion of solar energy will be absorbed at the outer surface of the metallic shell, thus acting as the "absorber". In these two mechanisms, the reflection coefficient $r$ for the first glass tube outer and inner surfaces, and that for the outer surface of the second tube, do not play a significant role. The reflection coefficient $r$ is known to be a function only of the incident angle and the refraction index of glass.

The absorption coefficients $a$ (for the first glass tube) and $\bar{a}$ (for the second glass tube) depend on the glass extinction coefficient $\phi$ and thickness $t$ (Ref. 5) such that

$$\left.\begin{aligned} a &= e^{-\phi t_f} \\ \bar{a} &= e^{-\bar{\phi} t_s} \end{aligned}\right\} \quad \text{or} \quad (2)$$

In general, the percentage of ferrous oxide ($F_2O_3$) in glass is important since iron accounts for most of the absorption. Reference 6 gives the extinction coefficient $\phi$ for the three different types of clear, medium-heat-absorbing and high-heat-absorbing glass panels as 6.85 $m^{-1}$, 129.92 $m^{-1}$, and 271.26 $m^{-1}$, respectively.

The reflectivity of the metallic shell $b$, on the other hand, affects the balance of heat absorbed, reflected, or transmitted to and from the second glass tube. The metallic shell outer surface can be either polished or coated to change the value of $b$, which will be shown next to be an important factor.

Several variations of the reflection coefficient $b$ were made in the program using the above three different types of second glass tube material. Both $T_c(0)$ and $T_A$ were set equal to isolate the effects of thermal losses and to focus on the collector optical efficiency alone. The results were plotted as shown in Fig. 6. Since the details of the optical properties of the collector components were not given by the manufacturer, the baseline collector properties were selected arbitrarily to be having a medium-heat-absorbing second glass tube ($\bar{\phi}$ = 129.92 $m^{-1}$), a polished copper shell ($b$ = 0.5), and a clear first glass tube ($\phi$ = 6.85 $m^{-1}$).

It can be observed from Fig. 6 that reducing the shell reflectivity $b$ always improves the optical efficiency with any type of second glass-material. The percentage improvement is large at small extinction coefficients. The collector efficiency for the first mechanism of heat transfer was found always higher than that for the second mechanism when both mechanisms have the same coefficient $b$. At small values of $b$, or at high shell absorptivity, the effect of $\phi$ becomes diminishing, and the collector optical efficiency reaches about 80%. This last result leads to the recommendation that high absorptivity or black coating is necessary for the metallic shell in order to achieve the highest performance, whether or not a heat-absorbing glass is used.

## E. Effect of Second Glass Tube Outer Surface Emissivity

If a "selective" coating is used on the outside surface of the second (inner) glass tube, it will reduce the outward infrared radiation losses, thus improving the performance. Different emissivity values were tested in the parameterization study, ranging from 0.05 to 0.9, with a reference value at 0.2, which is also "selective." The results are plotted as shown in Fig. 7. The strong relationship between the efficiency and the emissivity $\epsilon_s$ is clearly indicated in Fig. 7. The overall thermal loss coefficient $B_0$ is dominantly dependent on the "equivalent" radiation coefficient $B_4$, which is given in Eqs. (A-26) and (A-35). Smaller emissivity values cause smaller overall thermal loss coefficient, resulting in higher collector efficiency. If the infrared emissivity drops from the reference "selective" value ($\epsilon_s$ = 0.2) to a lesser emissivity value of 0.05, for example, i.e., a decrease of 75%, the overall thermal loss coefficient $B_0$ for the first collector unit will be decreased by 72% and the collector module efficiency will be improved by 24.1%. This is equivalent to a sensitivity of -0.32 for the collector module efficiency and +0.96 for the coefficient $B_0$. On the other hand, an increase of the emissivity ($\epsilon_s$) from 0.2 (selective) to 0.9 (flat black), i.e., an increase of 350% causes an increase in the loss coefficient $B_0$ for the first collector unit by 269% i.e., a loss coefficient sensitivity of 0.77. The corresponding module efficiency will drop to a low value of 10.4% i.e., a decrease of 78.9% compared to the reference state. The efficiency sensitivity in the latter case is equivalent to -0.22.

It can be concluded from the above discussion that "selective" coatings having an infrared emissivity in the order of 0.2 or less are recommended to achieve higher performance. Coating instability due to temperature recycling, aging, or operation at high temperatures and the associated increase in collector operation and maintenance cost, should be traded off against the improvement in collector performance.

## F. Effect of the Back Panel Reflectivity

The back reflector used, whether it is a V-shape or a cusplike shape, is necessary in order to enhance concentration of the solar flux on the glass tubes. Equation (A-11) gives the relationship between the augmentation factor $\lambda$ and the units spacing $S$, outer glass tube diameter $D_{f,o}$, and the back surface reflectivity ($\rho_v$). Equation (A-11) assumes that for both the V and cusp-back reflector types, the solar energy falling on the unshaded areas of the back reflector is reflected totally, with no loss, upon the external surface of the first glass tube. The higher the reflectivity $\rho_v$ is, the higher the augmentation factor, and the higher the efficiency will be. The results of varying $\rho_v$ are plotted in Fig. 8. The baseline design assumes a highly reflective mirrorlike material that is used for the back panel with $\rho_v$ of 0.9. If a polished aluminum rack with $\rho_v$ of 0.5, for example, is used, it means a drop in the reflectivity by 44.4%. The resulting drop in module efficiency is found to be 16.7%. This is equivalent to an efficiency sensitivity of about 0.38, which is not insignificant.

## G. Effect of Tubing Size

The size of the copper serpentine tube carrying the fluid is set using the manufacturer data to be a 6 mm (1/4 in.) nominal diameter. With a fluid flow of 50 kg/h, an inside diameter $D_{t,i}$ of 10 mm, and an outside diameter $D_{t,o}$ of 14 mm, the Reynolds number is computed as 6121, which lies in the transition region. Given a fixed mass flow rate, the effect of varying the tube diameter on the efficiency was studied for two different tube sizes. The first tubing has a nominal diameter of 1/8 in. ($D_{t,i}$ = 7.2 mm, $D_{t,o}$ = 10.2 mm) and the second tubing, has a nominal diameter of 3/8 in. ($D_{t,i}$ = 12.6 mm, $D_{t,o}$ = 17.2 mm). The resulting efficiencies were 49.50, 49.47, and 49.41%, corresponding to the nominal diameters of 1/8, 1/4, and 3/8 in., respectively.

The effect of tubing size could be considered, therefore, practically negligible. The slight improvement noticed above when a small tubing is used is contributed by the increased convective heat transfer coefficient $H_{ah}$ caused by the higher fluid velocities attained. The effect of the latter on performance was somewhat counterbalanced by the corresponding smaller heat transfer surface area.

## H. Effect of Fluid Mass Flow Rate

The choice of the operating mass flow rate is important if the collector efficiency needs to be improved and the pump horsepower to be decreased. Several references in the literature, including Ref. 7, have indicated a practical range from 24.4 kg/h-m$^2$ (5 lb/h-ft$^2$) to 97.7 kg/h-m$^2$ (20 lb/h-ft$^2$) to trade off between collector efficiency and pump horsepower. A recommended rate of 48.8 kg/h-m$^2$ (10 lb/h-ft$^2$) was given in Ref. 7. The flow rate recommended by the manufacturer for the 10-unit collector module is 50 kg/h or 34.2 kg/h-m$^2$ based on 1.464 m$^2$/module, which lies in the above practical range.

Increasing the fluid mass flow rate always increases the heat transfer between the copper tubing and the fluid, therefore increasing the extracted heat rate and the collector efficiency. On the other hand, for a given inlet fluid temperature, increasing the flow rate reduces the fluid exit temperature. Apart from the fact that a tradeoff analysis needs to be done with the feed pump horsepower, the "quality" of the extracted heat should be investigated from a thermodynamic availability viewpoint. If a reversible engine is connected to the collector and made to operate utilizing the collector extracted heat as if the latter is taken from a finite heat reservoir at the exit temperature $T_h(0)$, the availability $A$ will be as sketched in Fig. 9(a). $A$ is defined as the maximum useful mechanical work that could be obtained from the above collector-reversible engine system. $A$ is written for a constant specific heat fluid as

$$A = Q_{ext} - T_A MC_W \ln \frac{T_h(0)}{T_c(0)} \tag{3}$$

where

$$Q_{ext} = MC_w [T_h(0) - T_c(0)] \tag{4}$$

For a module with 10 units, the temperature $T_c(0)$ is taken at the entrance of the first unit and $T_h(0)$ is taken at the exit of the 10th unit. The relationship between the availability $A$ and the mass flow rate at given fluid inlet temperature $T_c(0)$ and ambient temperature $T_A$ has the same trend as sketched in Fig. 9(b). The values of peak availability $A_m^*$ at the optimum mass flow rate $M^*$ are plotted at different inlet fluid temperatures (Fig. 10). Figure 10 indicates that for given inlet fluid temperature and ambient temperature, there exists an optimum mass flow rate $M^*$ that corresponds to a maximum thermodynamic availability $A_m^*$. These findings are highly important in optimizing the collector operating conditions for solar-thermal-electric applications as will be shown in the next section.

## I. Effect of Inlet Fluid Temperature

The results of changing the cold fluid temperature at the entrance of the first collector unit are plotted as shown in Fig. 11. Increasing the temperature $T_c(0)$ causes an increase of the thermal losses from the collector surface since these losses are proportional to the temperature difference between the

collector operating temperature and ambient air. The correlation between $T_c(0)$ and the module efficiency tends to deviate from the approximate straight line form due to the increasing effect of the radiation losses at higher fluid temperatures. Although increasing, the inlet fluid temperature causes a setback in the collector efficiency; the resulting increase of the outlet fluid temperature may be favored, especially when the heat is converted to mechanical work via engines. In order to find the optimum inlet fluid temperature at which the production of mechanical work is maximum, the thermodynamic availability $A$ is introduced as in Eqs. (3) and (4). For a given mass flow rate, the availability $A$ was computed at different inlet temperatures, keeping all other variables unchanged. The peak availability $A_T^*$ and the optimum temperature $T_c^*(0)$ were registered at the given mass flow rate. The results were plotted as shown in Fig. 12. It is indicated from Fig. 12 that the maximum availability $A_T^*$, corresponding to the optimum inlet temperature, stays approximately constant if the flow rate is beyond 50 kg/h. The latter matches the flow rate recommended by the manufacturer. From Fig. 12, at a flow rate of 50 kg/h, the availability $A_T^*$ is maximum at an inlet fluid temperature of 69°C (156.2°F) and equal to 74.33 watts/module. On the other hand, entering the optimum fluid temperature (69°C) into Fig. 10, the optimum flow rate corresponding to a maximum availability $A_m^*$ is about 140 kg/h, where $A_m^*$ is about 74 watts/module. In general, maximizing the availability using the optimum inlet fluid temperature approach rather than the optimum mass flow rate approach is found convenient since the first gives more practical values of flow rates compared to the second approach.

## VI. Summary

In order to evaluate, in detail, the recently manufactured high-performance tubular collector by General Electric, a parameterization analysis was made. An in-house computer program was written for this purpose, following the thermodynamic analysis presented in Ref. 1 and the computational sequence in Appendices A and B. Comparison of simulated results and manufacturer's test data showed good agreement at a wide range of operating conditions. The comparison is considered a validation method for the computer program. Nine design and performance parameters were investigated to evaluate the performance sensitivity to their changes. The parameters considered were (1) solar radiancy, (2) wind speed, (3) ambient temperature, (4) reflectivity of metallic shell, (5) second tube outer surface emissivity, (6) reflectivity of back reflector, (7) fluid tubing size, (8) fluid mass flow rate, and (9) inlet fluid temperature to first collector unit. The results of this parameterization study shed some light onto variables of insignificant effects and others that need to be modified in the design in order to yield a higher performance than the present one.

# Definition of Terms

| | |
|---|---|
| $A$ | thermodynamic availability |
| $a, \bar{a}$ | glass absorption coefficient |
| $b$ | "absorber" reflection coefficient |
| $B_0$-$B_8$ | thermal conductance, W/m$^2$°C |
| $C$ | specific heat, W/kg°C |
| $C_0, C_1$ | constants |
| $D$ | diameter |
| $E_1$-$E_6$ | energy flux, W/m$^2$ |
| $F$ | flow factor |
| $G$ | heat capacity = $MC_w/D_{f,o}$ |
| $H$ | convective heat transfer coefficient, W/m$^2$°C |
| $I$ | solar flux, W/m$^2$ |
| $K$ | thermal conductivity, W/m°C |
| $L$ | collector-unit length, m |
| $M$ | fluid mass flow rate, kg/h |
| $N$ | number of collector units per module |
| $n$ | characteristic constant, m$^{-1}$ |
| $Q$ | heat rate, W |
| $R$ | equivalent radiation heat transfer coefficient, W/m$^2$°C |
| $r$ | glass reflection coefficient |
| $S$ | spacing between 2 consecutive collector units, m |
| $T$ | temperature, K |
| $t$ | thickness, m |
| $x$ | distance, m |
| $W$ | wind speed, m/s |
| $\alpha$ | absorptivity |
| $\rho$ | reflectivity |
| $\tau$ | transmissivity |
| $\lambda$ | augmented radiation factor |
| $\eta$ | collector efficiency |
| $\delta$ | parameter, °C/m |
| $\epsilon$ | emissivity |
| $\mu$ | viscosity |
| $\phi$ | extinction coefficient |

Subscripts

| | |
|---|---|
| $A$ | ambient air |
| $a$ | "absorber" metallic shell |
| $c$ | cold fluid |
| $e$ | effective |
| $f$ | first (outer) glass tube |
| $h$ | hot fluid |
| $i$ | inside |
| $o$ | outside |
| $s$ | second (inner) glass tube |
| $t$ | serpentine tube |
| $u$ | insulation |
| $v$ | V-shape reflector |
| $w$ | working fluid (hot or cold) |

# References


1. Lansing, F. L., and Yung, C. S., "A Two Dimensional Thermal Analysis of a New High Performance Tubular Solar Collector," in *The Deep Space Network Progress Report 42-49*, Jet Propulsion Laboratory, Pasadena, Calif., Feb. 15, 1979.
2. "SOLARTRON TC-100 Vacuum Tube Solar Collector – Commercial and Industrial Installation Manual," Document No. 78SDS4214A, General Electric Advanced Energy Programs, Philadelphia, Pa., Nov. 1978.
3. "SOLARTRON TC-100 Vacuum Tube Solar Collector – Commercial and Industrial Application Guide," Document No. 78SDS4215A, General Electric Advanced Energy Programs, Philadelphia, Pa., Nov. 1978.
4. Duffie, J. A., and Beckman, W. A., *Solar Energy Thermal Processes*, Wiley Interscience Publication, New York, N.Y., 1974.
5. Kreith, F., *Principles of Heat Transfer*, Third Edition, Intext Educational Publishers, New York, 1973.
6. Threlkeld, J. L., *Thermal Environmental Engineering*, Prentice-Hall, Inc., Englewood Cliffs, N.J., 1962.
7. Hewitt, H. C., and Griggs, E. I., "Optimal Mass Flow Rates Through Flat Plate Solar Collector Panels," ASME Publication 76-WA/SOL-19, presented at ASME Winter Annual Meeting, New York, N.Y., Dec. 1976.

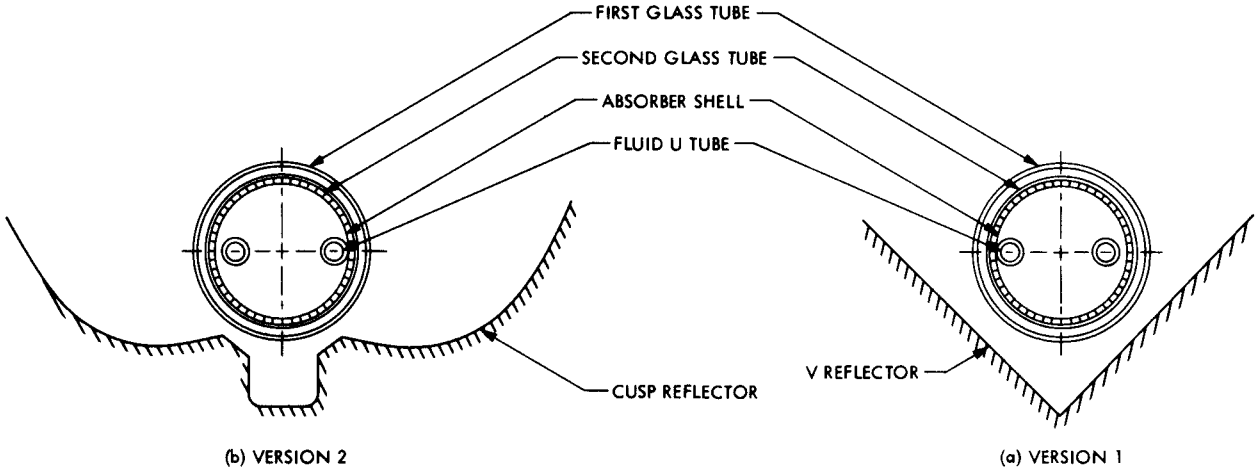


**Fig. 1. Two versions of a collector unit**

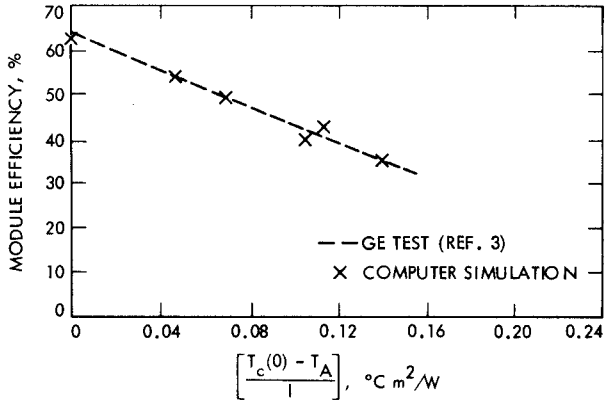


**Fig. 2. Performance comparison between some simulated and experimental data**

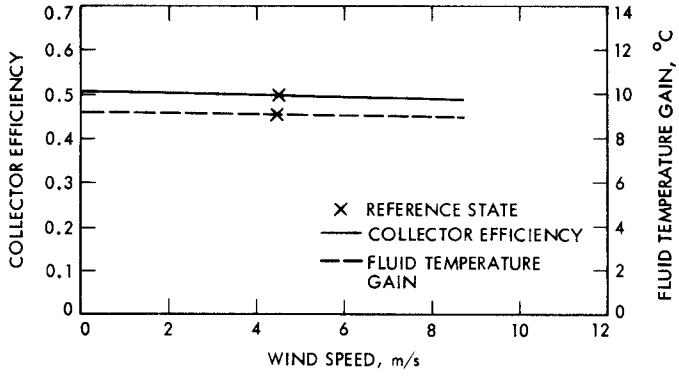


**Fig. 4. Effect of wind speed variations**

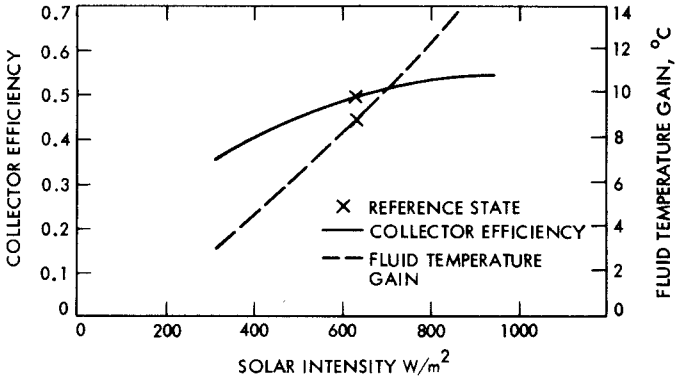


**Fig. 3. Effect of solar intensity variations**

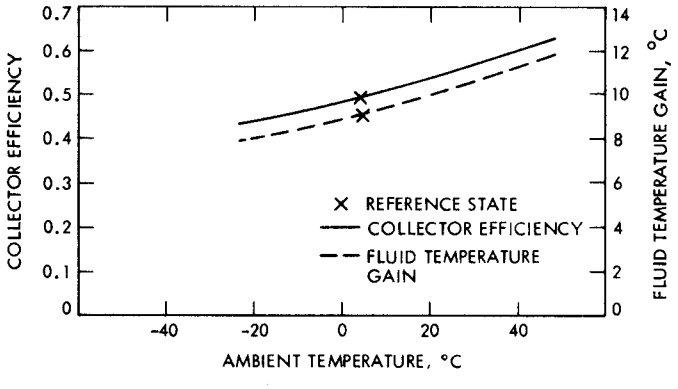


**Fig. 5. Collector performance vs ambient temperatures**

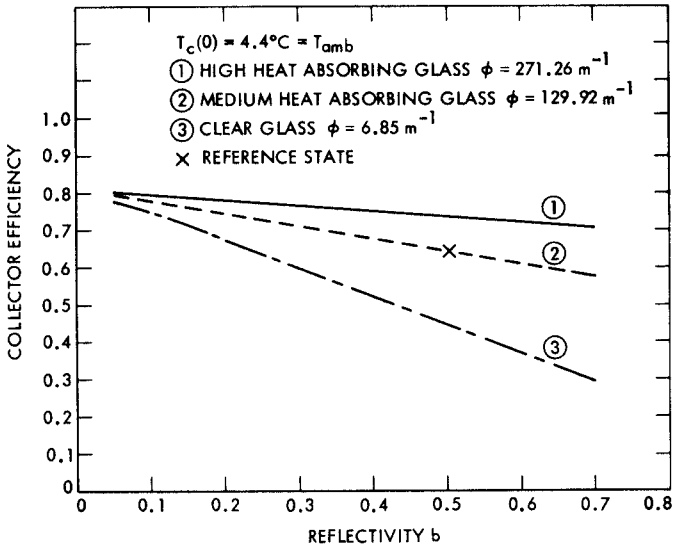


**Fig. 6. Effect of metallic shell reflectivity *b* on efficiency**

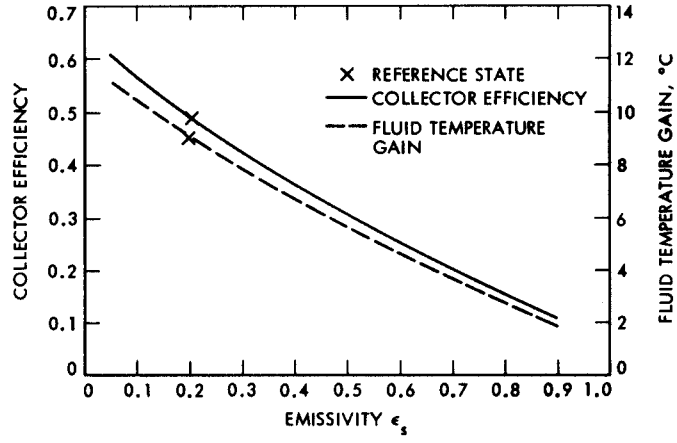


**Fig. 7. Effect of second glass surface emissivity $\epsilon_s$**

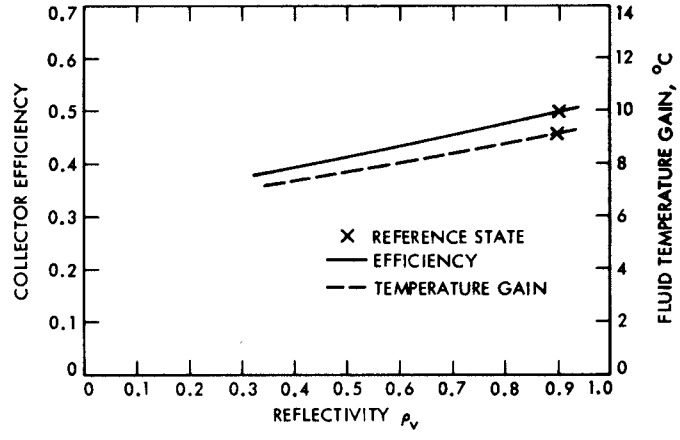


**Fig. 8. Effect of the reflectivity $\rho_v$ of the back V-shape reflector**

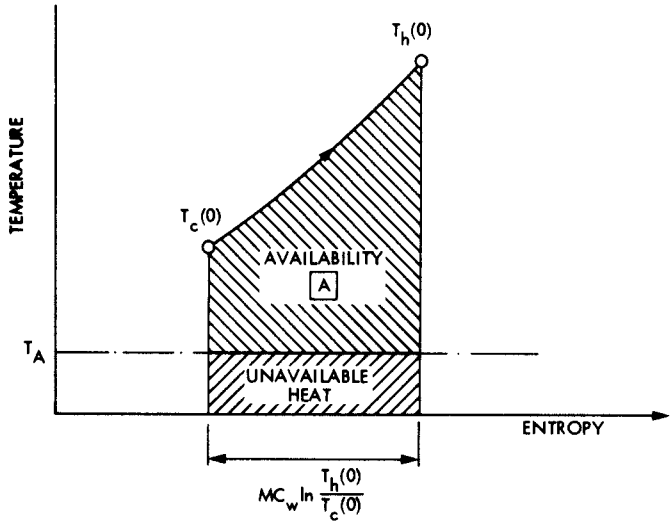


**Fig. 9a. Thermodynamic availability for the collector extracted heat**

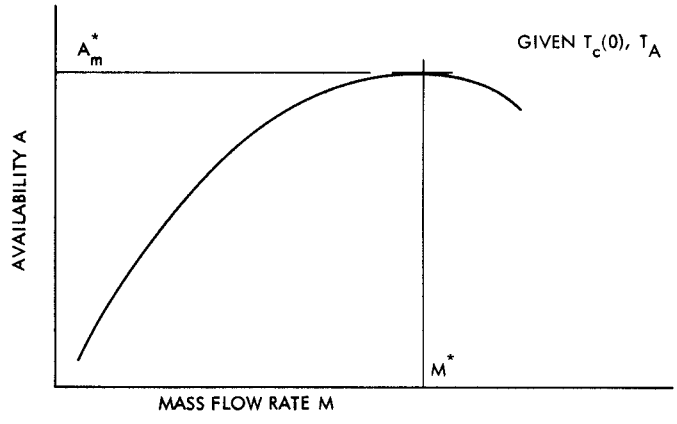


**Fig. 9b. Sketch of thermodynamic availability vs the mass flow rate for a given inlet and ambient temperature**

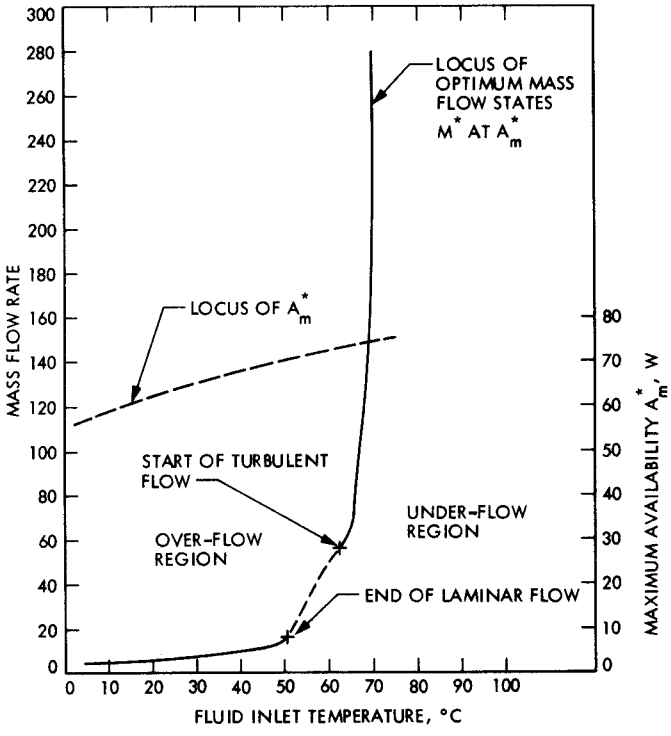


Fig. 10. Fluid inlet temperature effect on optimum mass flow rate

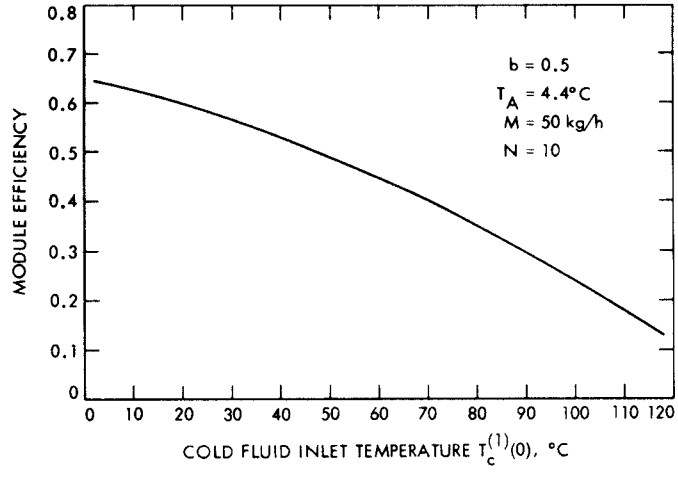


Fig. 11. Effect of inlet fluid temperature on module efficiency

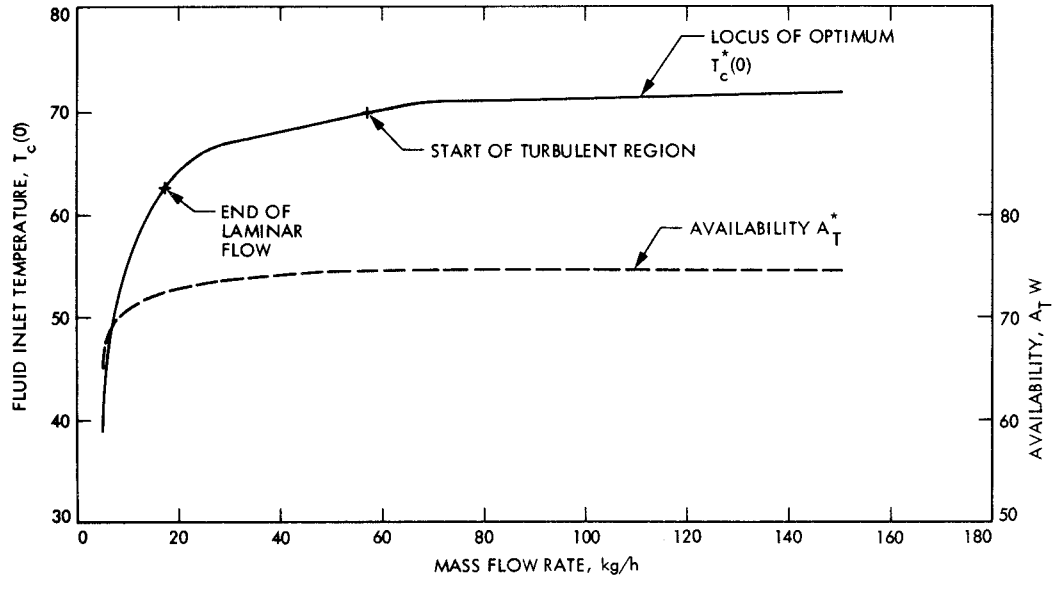


Fig. 12. Optimum fluid inlet temperature at various mass flow rates

# Appendix A

# Details of the Computer Model

## I. Introduction

A computer program is written using the thermal model and analytic equations given in the first phase of this study (Ref. 1). The program is divided into several parts described in detail next.

## II. Program Input Data

The following data need to be provided by the user in order to complete the program execution.

### A. Optical Properties

| | |
|---|---|
| Glass reflection coefficient | $r$ |
| First glass tube absorption (or extinction coefficient | $a$ (or $\phi$) |
| Second glass tube absorption (or extinction) coefficient | $\bar{a}$ (or $\bar{\phi}$) |
| Reflectivity of absorber shell | $b$ |
| Reflectivity of back reflector | $\rho_v$ |
| Emissivity of first glass tube surfaces | $\epsilon_f$ |
| Emissivity of second glass tube outer surface | $\epsilon_s$ |

### B. Collector Dimensions

| | |
|---|---|
| Spacing between collector units | $s$ |
| Inner diameter of first glass tube | $D_{f,i}$ |
| Outer diameter of first glass tube | $D_{f,o}$ |
| Inner diameter of second glass tube | $D_{s,i}$ |
| Outer diameter of second glass tube | $D_{s,o}$ |
| Inner diameter of metallic shell | $D_{a,i}$ |
| Outer diameter of metallic shell | $D_{a,o}$ |
| Inner diameter of fluid tubing | $D_{t,i}$ |
| Outer diameter of fluid tubing | $D_{t,o}$ |
| Length of one side of the U-tube of a collector unit | $L$ |
| Thickness of insulation at the open end | $t_u$ |
| Number of collector units per module | $N$ |

### C. Thermodynamic Properties

| | |
|---|---|
| Working fluid viscosity | $\mu_w$ |
| Working fluid specific heat | $C_W$ |
| Working fluid thermal conductivity | $K_W$ |
| Thermal conductivity of second glass tube | $K_s$ |
| Thermal conductivity of absorber metallic shell | $K_a$ |
| Thermal conductivity of open-end insulation | $K_u$ |

### D. Operating Conditions

| | |
|---|---|
| Fluid flow rate | $M$ |
| Fluid temperature at the entrance of the first collector unit | $T_c(0)$ |

### E. Weather

| | |
|---|---|
| Solar radiancy | $I$ |
| Ambient temperature (dry bulb) | $T_A$ |
| Wind speed | $W$ |

## III. Program Sequence

The following equations are listed in the same order of calculations sequence. Reference should be made to Ref. 1 for more details.

### A. Optical Properties

1. The transmissivity, absorptivity, and reflectivity of the first glass tube are $\tau_f$, $\alpha_f$ and $\rho_f$, respectively, where

$$\tau_f = \frac{a(1-r)^2}{1-a^2r^2} \tag{A-1}$$

$$\alpha_f = \frac{(1-r)(1-a)}{1-ar} \tag{A-2}$$

$$\rho_f = r + \frac{ra^2(1-r)^2}{1-a^2r^2} \tag{A-3}$$

where $r$ and $a$ are the reflection and absorption coefficients, respectively, for the first glass tube.

2. The absorptivity ($\alpha_B$) of the bottom surface of the second glass tube alone is given by

$$\alpha_B = \frac{\bar{a}(1-b)(1-r)}{1-\bar{a}^2 br} \tag{A-4}$$

Also, the absorptivity $\alpha_s$ and reflectivity $\rho_s$ of the second glass tube are given by

$$\alpha_s = \frac{(1-r)(1-\bar{a})(1+\bar{a}b)}{1-\bar{a}^2 br} \tag{A-5}$$

$$\rho_s = r + \frac{\bar{a}^2 b(1-r)^2}{1-\bar{a}^2 br} \tag{A-6}$$

where $\bar{a}$ and $r$ are the absorption and reflection coefficients of the second glass tube, and $b$ is the reflectivity of the absorber shell surface.

3. The effective properties $\alpha_{a,e}$ of the metallic absorber shell $\alpha_{f,e}$ and $\rho_{f,e}$ of the first glass tube and $\alpha_{s,e}$ of the second glass tube, are given by

$$\alpha_{a,e} = \frac{\alpha_B \tau_f}{1-\rho_f \rho_s} \tag{A-7}$$

$$\alpha_{f,e} = \alpha_f + \frac{\alpha_f \tau_f \rho_s}{1-\rho_f \rho_s} \tag{A-8}$$

$$\alpha_{s,e} = \frac{\alpha_s \tau_f}{1-\rho_f \rho_s} \tag{A-9}$$

$$\rho_{f,e} = \rho_f + \frac{\rho_s \tau_f^2}{1-\rho_f \rho_s} \tag{A-10}$$

4. Augmentation factor $\lambda$ is given by

$$\lambda = \left[1 + \rho_v \left(\frac{s}{D_{f,o}} - 1\right)\right] \tag{A-11}$$

## B. Heat Transfer Coefficients

**1. Convection coefficient between tubes and ambient.** The convective heat transfer coefficient between the outer glass tube and surrounding air, $H_{f_A}$ in W/m$^2$°C, is given approximately in Ref. 4 as a linear function of the wind speed $W$

$$H_{f_A} = 5.7 + 3.8W \tag{A-12}$$

where $W$ is in m/sec. Eq. (A-12) is also used to determine the film coefficients between the inner surface of "absorber" shell and the still air core $H_{aA}$, also between the end insulation and the air core $H_{uA}$. The coefficients are obtained by setting $W$ equal to zero in Eq. (A-12). Accordingly,

$$H_{aA} = H_{uA} \cong 5.7 \tag{A-13}$$

**2. Radiation coefficient.** Two "effective" radiation heat transfer coefficients are calculated for the present model, namely, $R_{sf}$ and $R_{f_A}$. The coefficient $R_{sf}$ represents the radiation exchange between the inner surface of the first (outer) glass tube and the outer surface of the second (inner) glass tube. Hence,

$$R_{sf} = \frac{\sigma\left(T_s^4 - T_f^4\right)}{\left[(T_s - T_f)\left(\frac{1}{\epsilon_s} + \left(\frac{1}{\epsilon_f} - 1\right)\frac{D_{s,o}}{D_{f,i}}\right)\right]} \tag{A-14}$$

The coefficient $R_{f_A}$ represents the radiation exchange between the first (outer) glass tube and the ambient air and is given by

$$R_{f_A} = \frac{\epsilon_f \sigma\left(T_f^4 - T_A^4\right)}{(T_f - T_A)} \tag{A-15}$$

A convergent iterative process is used for each collector unit whereby average temperatures of each of the first glass tubes are assumed. These averages give the first estimate of the coefficients $R_{sf}$ and $R_{f_A}$ to determine the temperature distribution $T_f(x)$ and $T_s(x)$ which in turn are used to modify the radiation coefficients. The iteration process is completed for a given collector unit before proceeding to the next unit in the module and so on.

**3. Convection between the working fluid and tubes.** The present model incorporates all the equations needed to calculate the forced convection heat transfer coefficient between the working fluid and the copper tubing at any one of the three flow regions: laminar, transition, and turbulent. The laminar region is characterized by a Reynolds number (Re) less than 2100 for circular tubes. For the turbulent flow case, the Reynolds number is greater than 7000. References 4 and 5

were used to determine the Nusselt number (Nu) for laminar and turbulent flow regions. For laminar flow

$$Nu = 4.64 + \frac{0.067\, D_{t,i}\, Re\, Pr/l}{1 + 0.04 \left(\frac{D_{t,i}}{l} Re\, Pr\right)^{2/3}} \qquad \text{(A-16)}$$

where $D_{t,i}$ is the inner tube diameter, $l$ is the total tube length and $Pr$, $Re$ and $Nu$ are Prandtl, Reynolds, and Nusselt numbers, respectively. The dimensionless numbers are written as follows:

$$\left.\begin{aligned} Re &= \frac{4M}{\pi D_{t,i} \mu_W} \\ Pr &= \frac{C_W \mu_W}{K_W} \\ Nu &= \frac{H_{ah} D_{t,i}}{K_W} \end{aligned}\right\} \qquad \text{(A-17)}$$

For turbulent flow inside tubes, the Nusselt number $Nu$, is given by

$$Nu = 0.023\, Re^{0.8}\, Pr^{0.3} \qquad \text{(A-18)}$$

In the metastable transition region, no reliable expression has been found in the literature to express the Nusselt number. Accordingly, a linear interpolation is used in this work as a first approximation of the fluid transition from laminar to turbulent regions, i.e., in the range where $2100 < Re < 7000$. The approximate equation used is

$$Nu_{\text{(transition)}} = Nu_{2100} + (Re - 2100)\left(\frac{Nu_{7000} - Nu_{2100}}{7000\text{-}2100}\right) \qquad \text{(A-19)}$$

where $Nu_{2100}$ is the Nusselt number computed from Eq. (A-16) at $Re$ equal to 2100 and $Nu_{7000}$ is the Nusselt number computed from Eq. (A-18) at $Re$ equal to 7000.

The fluid thermal properties used in the above equations were taken at some preselected average bulk temperature and were assumed to be constant during operation. The working fluid used in the modelling exercise was the ethylene glycol-water solution with a volumetric ratio of 50/50 as recommended by the manufacturer. Pure water was not selected because of its inadequacy at working temperatures below 0°C (32°F) or above 100°C (212°F).

## C. Absorbed Energy Flux *E* Coefficients

The energy flux terms ($E$'s), discussed in detail in Ref. 1, are rewritten here to complete the program sequence.

1. The fraction of solar energy that is absorbed by the "absorber" shell $E_1$ is given by

$$E_1 = \alpha_{a,e}\, \lambda\, I \qquad \text{(A-20)}$$

2. The fraction of solar energy that is absorbed by the first (outer) glass tube $E_2$ is expressed by

$$E_2 = \alpha_{f,e}\, \lambda\, I \qquad \text{(A-21)}$$

3. The fraction of solar energy that is absorbed by the second (inner) glass tube $E_3$ is written as

$$E_3 = \alpha_{s,e}\, \lambda\, I \qquad \text{(A-22)}$$

## D. "Equivalent" Heat Transfer Coefficients (*B*'s)

The $B$ coefficients are herein called "equivalent" since they represent the "equivalent" heat transfer coefficients for a plate-to-plate heat exchange giving the same heat transfer of the present circular geometry. The $B$ coefficients were previously discussed in Ref. 1 and are rewritten here, briefly, for completion.

1. The "equivalent" conduction coefficient $B_1$ between the "absorber" shell and second (inner) glass tube is given by

$$B_1 = \frac{2\pi/D_{f,o}}{\left[\frac{ln\,(D_{s,o}/D_{s,i})}{K_s} + \frac{ln\,(D_{a,o}/D_{a,i})}{K_a}\right]} \qquad \text{(A-23)}$$

2. The coefficient $B_2$ represents the "equivalent" heat loss coefficient from the central air core to the ambient air through the open and closed ends of the collector. Figure A-1 shows a sketch of the location of film coefficients used in deriving the $B_2$ expression for one collector unit having one end insulated and the other using double hemispheres with vacuum in between. One can prove that

$$B_2 = \frac{1}{\left[\frac{D_{f,o}}{\pi h_{aA}(D_{a,i} + 2D_{t,o})} + \frac{1}{PA_c}\right]} \qquad \text{(A-24)}$$

where $P$ and $A_c$ are given by

$$P = \frac{2}{\frac{1}{H_{aA}} + \frac{1}{R_{sf}} + \frac{2\,t_s}{K_s} + \frac{1}{H_{f_A}}} + \frac{1}{\frac{1}{H_{uA}} + \frac{t_u}{K_u} + \frac{1}{H_{fA}}}$$

$$A_c = \frac{\pi}{4} D_{a,i}^2$$

3. The "equivalent" convection coefficient between the absorber shell and the fluid ($B_3$) is given by

$$B_3 = \pi\,(D_{t,i}/D_{f,o})\,H_{ah} \qquad \text{(A-25)}$$

4. The "equivalent" radiation coefficient between the first glass and second glass tubes is given by

$$B_4 = \pi\,R_{sf}\,(D_{s,o}/D_{f,o}) \qquad \text{(A-26)}$$

5. The "equivalent" combined radiation and convection coefficient between the first glass tube and ambient is written as

$$B_5 = \pi\,(H_{fA} + R_{fA}) \qquad \text{(A-27)}$$

## E. Overall Heat Loss Coefficient $B_0$

The coefficients $B_1$, $B_2$, $B_4$, and $B_5$ represent, by analogy to electric circuits, the thermal conductances between the "absorber" shell, glass tubes and ambient air as shown in Fig. A. The thermal resistances $1/B_1$, $1/B_4$, and $1/B_5$ are connected in series and their resultant is connected in parallel with the resistance $1/B_2$. The overall thermal conductance of this circuit is herein called the overall heat loss coefficient $B_0$ given by

$$B_0 = B_2 + \frac{1}{\frac{1}{B_1} + \frac{1}{B_4} + \frac{1}{B_5}}$$

## F. Temperature Distribution

The hot and cold temperatures $T_h(x)$ and $T_c(x)$, respectively, at any position $x$ from the open end of one collector unit, are obtained from

$$T_h(x) = \frac{\delta}{C_1 - C_0} - \left[\frac{\delta}{C_1 - C_0} - T_c(0)\right] \left[\frac{n\cosh n(L-x) - (C_1 - C_0)\sinh n(L-x)}{n\cosh nL + (C_1 - C_0)\sinh nL}\right] \qquad \text{(A-28)}$$

$$T_c(x) = \frac{\delta}{C_1 - C_0} - \left[\frac{\delta}{C_1 - C_0} - T_c(0)\right] \left[\frac{n\cosh n(L-x) + (C_1 - C_0)\sinh n(L-x)}{n\cosh nL + (C_1 - C_0)\sinh nL}\right] \qquad \text{(A-29)}$$

where the constants $n$, $c_0$, $c_1$ and $\delta$ are computed in sequence from the following equation:

$$\left.\begin{aligned} n &= \sqrt{C_1^2 - C_0^2} \\ C_0 &= B_3^2/(GB_8) \\ C_1 &= \frac{B_3}{GB_8}(B_8 - B_3) \\ \delta &= B_3\,E_6/GB_8 \end{aligned}\right\} \qquad \text{(A-30a)}$$

where

$$\left.\begin{aligned} E_6 &= E_1 + B_2\,T_A + \frac{B_1\,E_5}{B_7} \\ E_5 &= E_3\frac{B_6}{B_1} + E_4\frac{B_4}{B_1} \\ E_4 &= E_2 + B_5\,T_A \end{aligned}\right\} \qquad \text{(A-30b)}$$

$$\left.\begin{aligned} B_8 &= B_2 + 2B_3 + \frac{B_4\,B_5}{B_7} \\ B_7 &= B_6 + \frac{B_4\,B_5}{B_1} \\ B_6 &= B_4 + B_5 \end{aligned}\right\} \qquad \text{(A-30c)}$$

and

$$G = \frac{M\,C_W}{D_{f,o}} \qquad \text{(A-30d)}$$

The "absorber" shell temperature $T_a(x)$ is given by

$$T_a(x) = \frac{\{E_6 + B_3\,[T_h(x) + T_c(x)]\}}{B_8} \qquad \text{(A-31)}$$

The second glass tube temperature $T_s(x)$ is given by

$$T_s(x) = \frac{[E_5 + B_6\, T_a(x)]}{B_7} \qquad \text{(A-32)}$$

Also, the first glass tube temperature $T_f(x)$ is given by

$$T_f(x) = \frac{[E_4 + B_4\, T_s(x)]}{B_6} \qquad \text{(A-33)}$$

## G. Performance Factors

The flow factor $F$ is defined by

$$F = \frac{GD_{f,o}}{SL\, B_0}\left[\frac{2 \sinh nL}{\frac{B_3}{nG}\cosh nL + \sinh nL}\right] \qquad \text{(A-34)}$$

where $B_0$ is the overall heat loss coefficient given in Sec. A.3.5. by

$$B_0 = B_2 + \frac{B_4 B_5}{B_7} = B_2 + \frac{1}{\frac{1}{B_1} + \frac{1}{B_4} + \frac{1}{B_5}} \qquad \text{(A-35)}$$

The unit collector instantaneous efficiency, based on the solar radiancy falling on the projected area $SL$ is given by

$$\eta_{unit} = \frac{MC_w\,[T_h(0) - T_c(0)]}{ISL}$$

or

$$\eta_{unit} = F\left[\lambda\left(\alpha_{a,e} + \alpha_{f,e}\frac{B_4}{B_7} + \alpha_{s,e}\frac{B_6}{B_7}\right) - B_0\frac{T_c(0) - T_A}{I}\right] \qquad \text{(A-36)}$$

where $SL$ is the projected area of a collector unit. For a collector module that consists of $N$ collector units in series, the module efficiency is given by

$$\eta_{module} = \frac{MC_w\,[T_h^{(N)}(0) - T_c^{(1)}(0)]}{ISLN} \qquad \text{(A-37)}$$

where $T_h^{(N)}(0)$ is the fluid temperature at the exit of the $n$th unit and $T_c^{(1)}(0)$ is the fluid temperature at the entrance of the first collector unit.

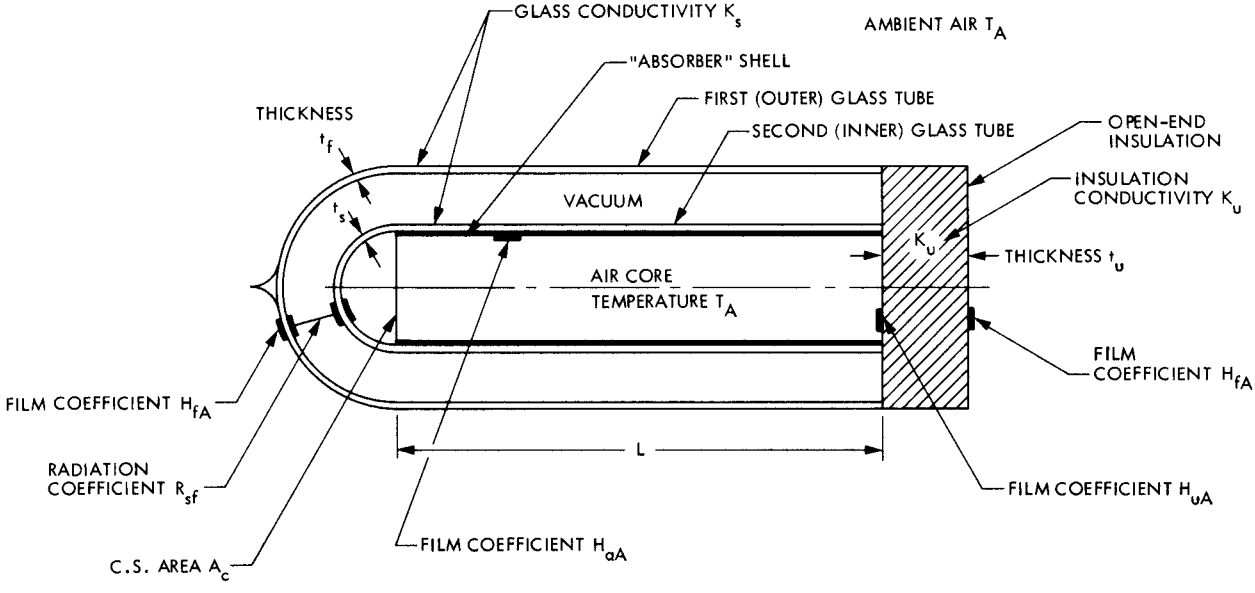


**Fig. A-1. Film coefficients used for the determination of the "equivalent" coefficient $B_2$**

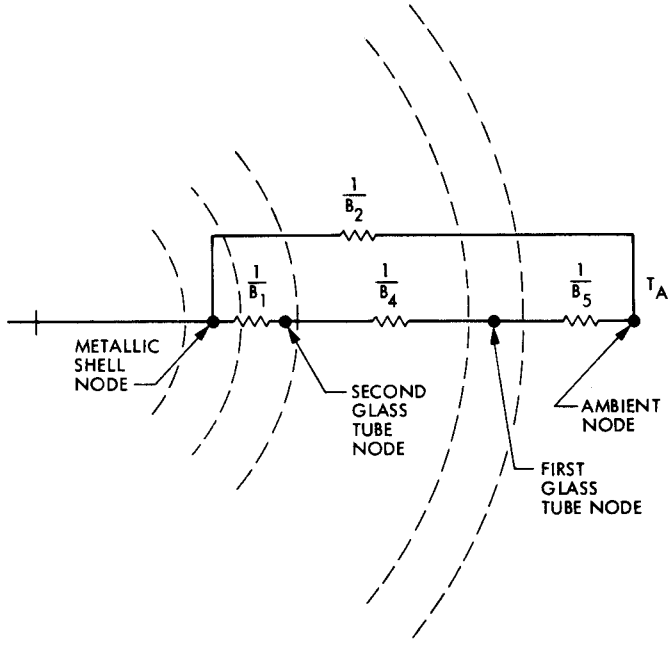


**Fig. A-2. Overall heat loss coefficient $B_0$**

# Appendix B
# Numerical Example

As an illustration of the use of the computer program described in Appendix A, a numerical example is given next to show the sequence followed. For convenience, the performance of only one collector unit will be computed. The performance of a module with $N$ units in series can be computed by repetition, following the same sequence of calculations of a single unit.

## I. Input Variables

The following input variables are entered in the program where some were based on information provided by the manufacturer and the rest were estimated from past experience. The input data are grouped in order similar to Section II of Appendix A.

### A. Optical Properties

| | |
|---|---|
| Glass reflection[1] coefficient $r$ | 0.043 |
| First glass tube extinction[2] coefficient $\phi$ | 6.85 $m^{-1}$ |
| Second glass tube extinction[3] coefficient $\phi$ | 129.92 $m^{-1}$ |
| Reflectivity[4] of metallic shell $b$ | 0.5 |
| Reflectivity[5] of back V-reflector $\rho_v$ | 0.9 |
| Emissivity of first glass tube surfaces $\epsilon_f$ | 0.9 |
| Emissivity[6] of second glass tube surface $\epsilon_s$ | 0.2 |

### B. Collector Dimensions

| | |
|---|---|
| Spacing[7] between two consecutive collector units $S$ | 0.12 m |
| Inner diameter[8] of first glass tube $D_{f,i}$ | 0.076 m |
| Outer diameter[8] of first glass tube $D_{f,o}$ | 0.082 m |
| Inner diameter[8] of second glass tube $D_{s,i}$ | 0.058 m |
| Outer diameter[8] of second glass tube $D_{s,o}$ | 0.064 m |
| Inner diameter[8] of metallic shell $D_{a,i}$ | 0.056 m |
| Outer diameter[8] of metallic shell $D_{a,o}$ | 0.058 m |
| Length of one[8] side of U-tube $L$ | 1.22 m |
| Thickness[8] of insulation at the open end $t_u$ | 0.004 m |

### C. Thermodynamic Properties

| | |
|---|---|
| Type of working fluid: ethylene glycol-water (50/50) by volume | |
| Fluid viscosity[9] $\mu_w$ | 1.04 kg/m h |
| Fluid specific heat[9] $C_w$ | 1.0122 Wh/kg°C |
| Fluid thermal conductivity[9] $K_w$ | 0.4 W/m°C |
| Glass thermal conductivity $K_s$ | 0.7 W/m°C |
| Thermal conductivity of shell $K_a$ | 380.16 W/m°C |
| Thermal conductivity of open-end insulation $K_u$ | 0.319 W/m°C |

### D. Operating Conditions

| | |
|---|---|
| Fluid flow rate, m | 5.0 kg/h |
| Inlet fluid temperature $T_c(0)$ | 48.89°C (120°F) |

### E. Weather

| | |
|---|---|
| Solar radiancy $I$ | 630.7 W/m² (200 Btu/h ft²) |
| Ambient temperature $T_A$ | 4.4°C (40°F) |
| Wind speed $W$ | 4.47 m/s (10 mph) |

## II. Output Results

The following is a partial list of the output results obtained from running the computer program using Sec. B.1 data.

### A. Optical Properties

| | | |
|---|---|---|
| $\alpha_f$ | (Eq. A-2) | 0.0203 |
| $\alpha_{f,e}$ | (Eq. A-8) | 0.0251 |
| $\alpha_s$ | (Eq. A-5) | 0.4176 |
| $\alpha_{s,e}$ | (Eq. A-9) | 0.3833 |

[1] Taken at zero incidence angle and a glass refraction index of 1.526.
[2] Assumed made of clear glass (Refs. 2 and 3).
[3] Assumed made of a medium heat absorbing glass.
[4] For polished copper surface.
[5] For silvered aluminum surface.
[6] Assumed for a selective coating.
[7] See Refs. 2 and 3.
[8] Estimated from sketches in Refs. 2 and 3.
[9] Taken as an average from 4°C to 120°C.

| | | |
|---|---|---|
| $\alpha_B$ | (Eq. A-4) | 0.3273 |
| $\alpha_{a,e}$ | (Eq. A-7) | 0.3004 |
| $\lambda$ | (Eq. A-11) | 1.4171 |

### B. Heat Transfer Coefficients

| | |
|---|---|
| Reynolds number Re | 612.1 (laminar) |
| Prandtl number Pr | 2.632 |
| Nusselt number Nu | 4.748 |
| Fluid heat transfer coefficient $H_{ah}$ | 189.9 W/m$^2$°C |
| "Equivalent" coefficient $B_1$ | 544.5117 W/m$^2$°C |
| "Equivalent" coefficient $B_2$ | 0.1336 W/m$^2$°C |
| "Equivalent" coefficient $B_3$ | 72.7588 W/m$^2$°C |
| "Equivalent" coefficient $B_4$ | 3.1424 W/m$^2$°C |
| "Equivalent" coefficient $B_5$ | 85.1437 W/m$^2$°C |
| Overall loss coefficient $B_0$ | 3.1473 W/m$^2$°C |

### C. Temperature Distribution

The temperature profile along each collector tube is plotted as shown in Fig. B-1 at the above input conditions. The arithmetic average of the tube temperatures are as follows: 6.58°C for the first glass tube; 58.57°C for the second glass tube; 58.24°C for the metallic shell; 53.05°C for the cold fluid and 57.38°C for the hot fluid. The actual fluid temperature gain $[T_h(0) - T_c(0)]$ is computed as 8.6996°C using Eqs. (A-28) and (A-29).

In addition to the above results, the flow factor $F$ is computed as 0.6401 and the collector efficiency is found to be 47.68%.

## III. Temperature Trends for Hot and Cold Fluids

The hot and cold fluid temperatures $T_h(x)$ and $T_c(x)$ were given in Appendix A by Eqs. (A-28) and (A-29), respectively. The useful temperature gain $[T_h(x) - T_c(x)]$ at any position $x$ from the open end can be written as

$$[T_h(x) - T_c(x)] = \left[\frac{\delta}{C_1 - C_0} - T_c(0)\right] \left[\frac{2(C_1 - C_0)\sinh n(L - x)}{n\cosh nL + (C_1 - C_0)\sinh nL}\right] \quad \text{(B-1)}$$

To find the location of any maximum or minimum fluid temperatures along the collector length, Eqs. (A-28), (A-29), and (B-1) are differentiated with respect to ($x$) keeping all other parameters constant. One can prove mathematically that neither the cold temperature $T_c(x)$ nor the useful temperature gain $[T_h(x) - T_c(x)]$ can ever possess any maximum or minimum value. In spite of this finding, the hot fluid temperature $T_h(x)$ possesses one peak value at some location $\bar{X}$ (measured from the open end) given by

$$\bar{X} = L - \frac{1}{n}\tanh^{-1}\left(\frac{C_1 - C_0}{n}\right) \quad \text{(B-2)}$$

$\bar{X}$ can be either within the collector tube or theoretically outside $0 \leqslant x \leqslant L$ depending on the constants $C_1$, $C_0$. The corresponding temperature difference $[T_h(\bar{X}) - T_c(\bar{X})]$ can be proven to be smaller than that at the open end ($x = 0$) at all times. The conclusion is that the rate of energy extracted from the collector is maximum at the open end and is unaffected by the internal temperature peaks. The optical stability of selective coatings, on the other hand, is related to the highest temperature attained, and therefore needs this investigation.

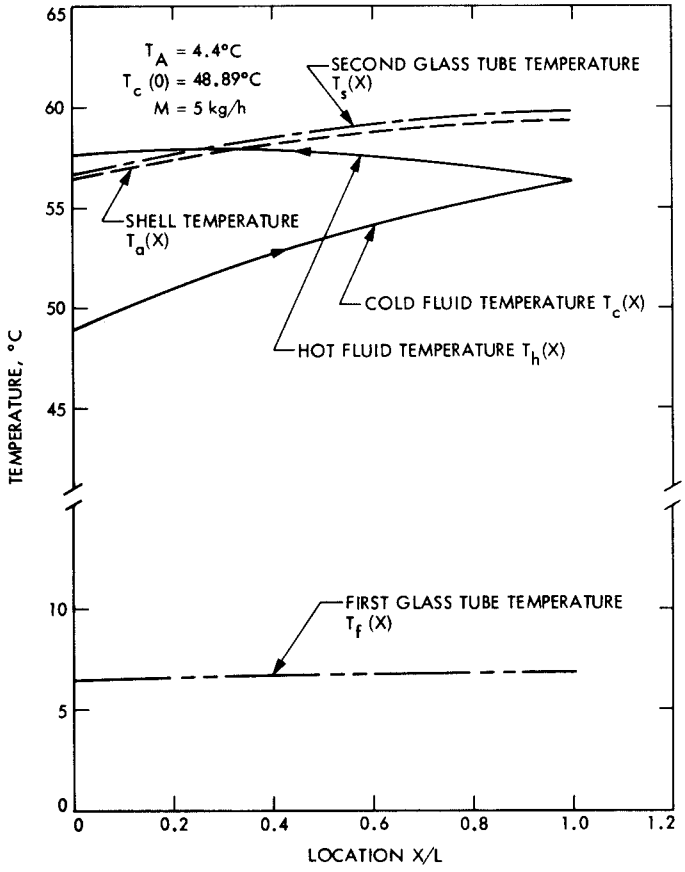


**Fig. B-1. Temperature distribution along a collector unit**